THE JOURNAL OF PHYSICAL CHEMISTRY A

Article

pubs.acs.org/JPCA

# Infrared Spectra of the 1-Pyridinium ($C_5H_5NH^+$) Cation and Pyridinyl ($C_5H_5NH$ and 4-$C_5H_6N$) Radicals Isolated in Solid *para*-Hydrogen

Barbara Golec,[†] Prasanta Das,[†] Mohammed Bahou,[†] and Yuan-Pern Lee*[,†,‡]

[†]Department of Applied Chemistry and Institute of Molecular Science, National Chiao Tung University, Hsinchu 30010, Taiwan

[‡]Institute of Atomic and Molecular Sciences, Academia Sinica, Taipei 10617, Taiwan

Supporting Information

**ABSTRACT:** Protonated pyridine and its neutral counterparts ($C_5H_6N$) are important intermediates in organic and biological reactions and in the atmosphere. We have recorded the IR absorption spectra of the 1-pyridinium ($C_5H_5NH^+$) cation, 1-pyridinyl ($C_5H_5NH$), and 4-pyridinyl (4-$C_5H_6N$) produced on electron bombardment during matrix deposition of a mixture of pyridine ($C_5H_5N$) and *p*-$H_2$ at 3.2 K; all spectra were previously unreported. The IR features of $C_5H_5NH^+$ diminished in intensity after the matrix was maintained in darkness for 15 h, whereas those of $C_5H_5NH$ and 4-$C_5H_6N$ radicals increased. Irradiation of this matrix with light at 365 nm diminished lines of $C_5H_5NH^+$ and $C_5H_5NH$ but enhanced lines of 4-$C_5H_6N$ slightly, whereas irradiation at 405 nm diminished lines of 4-$C_5H_6N$ significantly. Observed wavenumbers and relative intensities of these species agree satisfactorily with the anharmonic vibrational wavenumbers and IR intensities predicted with the B3LYP/6-31++G(d,p) method. Assignments of $C_5H_5NH$ and 4-$C_5H_6N$ radicals were further supported by the observation of similar spectra when a $Cl_2/C_5H_5N/p$-$H_2$ matrix was irradiated first at 365 nm and then with IR light to generate H atoms to induce the H + $C_5H_5N$ reaction.

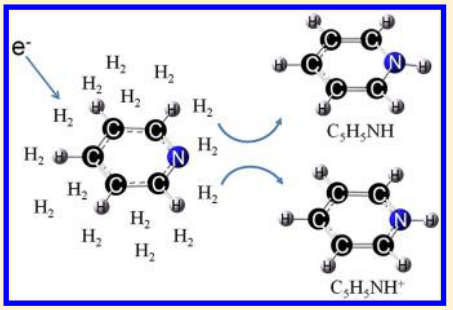


## 1. INTRODUCTION

Pyridine ($C_5H_5N$) is an important solvent and reagent in organic synthesis and also a precursor widely used for agrochemical and pharmaceutical compounds. The reaction of pyridine with acids leads to formation of the pyridinium cation ($C_5H_6N^+$).[1] Because pyridine is emitted into the atmosphere as the result of coal combustion and other industrial activities, the pyridinium cation and its derivatives have been observed in a significant proportion in the lower troposphere.[2−4] The pyridinium ion also plays an important role in Friedel−Crafts acylation; when pyridine is employed in the reaction, the pyridinium ion forms a complex with the electrophilic acylium ion, rendering it more reactive.[5] The photoinduced proton transfer in a pyridine-based polymer gel, a candidate for light-sensitive memory devices and optical switches, is responsible for its structural changes.[6] The neutralization of pyridinium cations results in formation of pyridinyl radicals ($C_5H_6N$). Both pyridinium cation and pyridinyl radical were suggested as intermediates in the hydrogenation of pyridine on metal surfaces.[7,8]

Pyridinium cations have four isomeric forms, shown in Figure 1, with the proton attached to the N atom of pyridine (1-$C_5H_6N^+$, designated $C_5H_5NH^+$) or to the carbon atom at ortho, meta, or para positions of the pyridine ring, designated 2-$C_5H_6N^+$, 3-$C_5H_6N^+$, or 4-$C_5H_6N^+$, respectively. The protonation of pyridine was a subject of numerous experimental investigations,[1,7−10] but only $C_5H_5NH^+$ was positively identified. This observation is consistent with theoretical calculations that predicted $C_5H_5NH^+$ as the most stable isomer; the 2-, 3-, and 4-$C_5H_6N^+$ isomers were predicted to be greater in energy than $C_5H_5NH^+$ by 266, 238, and 287 kJ $mol^{-1}$, respectively, with the MP2/6-311G(2d,p) method.[1] The experimentally determined enthalpy of formation of $C_5H_5NH^+$ is 746 kJ $mol^{-1}$.[11] The experimentally determined proton affinity of pyridine at 298 K is 930 kJ $mol^{-1}$,[12] consistent with values 921−937 kJ $mol^{-1}$ predicted using various methods.[1,13,14]

The ultraviolet (UV) spectra of $C_5H_6N^+$ in an aqueous solution show absorption bands near 201, 251, 256, and 261 nm.[15] The reported infrared (IR) absorption bands of $C_5H_6N^+$ are derived mostly from the pyridinium salts in their solid state,[16] in solutions,[17−20] in zeolites,[9,21] or on a Pt surface;[7,8] these spectra might be strongly perturbed by nearby molecules or ions. Nguyen and Tureček predicted vibrational wavenumbers of various isomers of $C_5H_6N^+$,[1] but no IR spectrum of isolated pyridinium cations, either in the gaseous phase or in matrices, has been reported.

The pyridinyl radicals, $C_5H_6N$, have four isomers with the hydrogen atom attached to the nitrogen atom (1-$C_5H_6N$, designated $C_5H_5NH$ in this paper) or to one carbon atom at ortho, meta, or para positions of the pyridine ring, designated 2-$C_5H_6N$, 3-$C_5H_6N$, or 4-$C_5H_6N$, respectively, as shown in Figure 2. At 0 K, the energies of 2-$C_5H_6N$ and 3-$C_5H_6N$

**Special Issue:** Terry A. Miller Festschrift

**Received:** August 1, 2013
**Revised:** September 10, 2013
**Published:** September 11, 2013

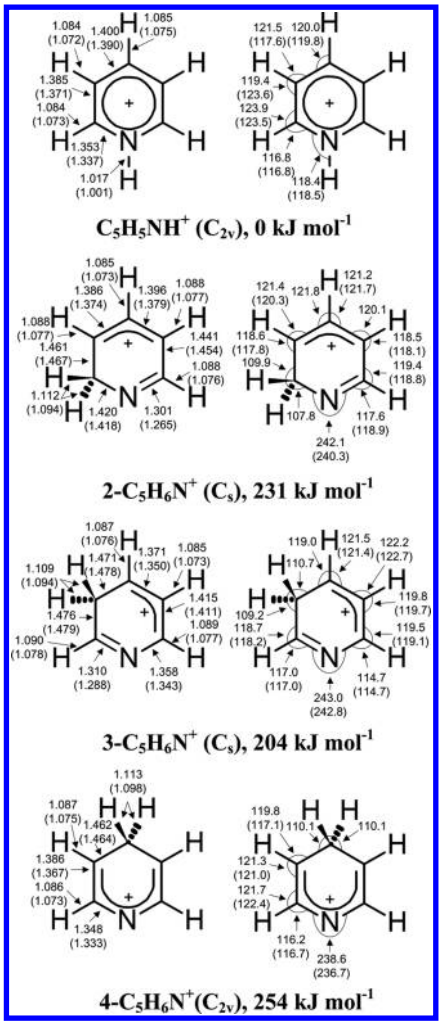


**Figure 1.** Geometries and relative energies (corrected for zero-point vibrational energy) of isomers of pyridinium ($C_5H_6N^+$) cations calculated with the B3LYP/6-31++G(d,p) method. Bond distances are in Å and bond angles in degree. Literature values predicted with the RHF/6-31G(d,p) method[1] are listed parenthetically.

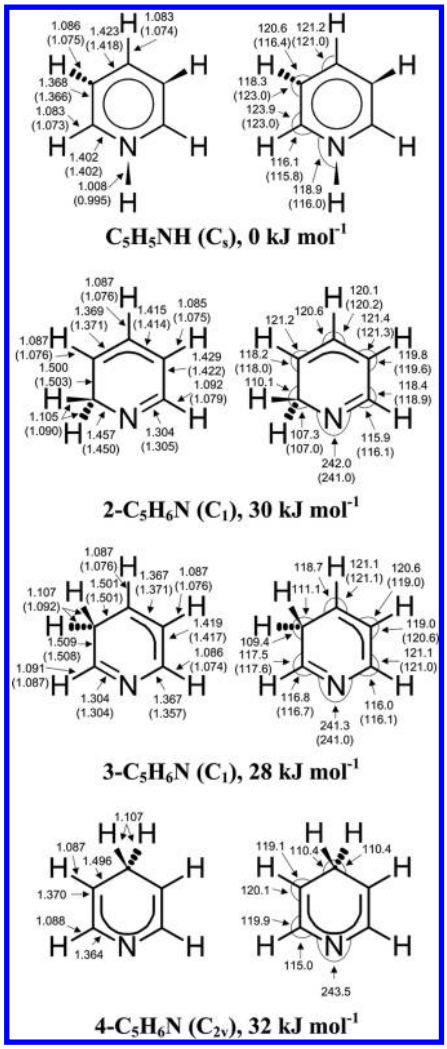


**Figure 2.** Geometries and relative energies (corrected for zero-point vibrational energy) of isomers of pyridinyl ($C_5H_6N$) radicals calculated with the B3LYP/6-31++G(d,p) method. Bond distances are in Å and bond angles in degree. Literature values predicted with the UHF/6-31G(d,p) method[1] are listed parenthetically.

radicals were predicted to be ~30 and 25 kJ mol$^{-1}$ greater than that of $C_5H_5NH$ at the MP2/6-311G(2d,p) level of theory.[1] Cercek and Ebert employed pulsed radiolysis to estimate the molar absorption coefficient at 275 nm for $C_5H_5NH$ in an aqueous solution to be 1800 dm$^3$ mol$^{-1}$ cm$^{-1}$.[22] The electron paramagnetic resonance (EPR) spectrum of pyridine at pH = 12.1 indicates that the structure of the pyridinyl radical is $C_5H_5NH$.[23] Nguyen and Tureček predicted vibrational wavenumbers of $C_5H_5NH$, 2-$C_5H_6N$, and 3-$C_5H_6N$,[1] but no IR spectrum of pyridinyl radical in any isomeric form has been reported.

The use of solid *para*-hydrogen (*p*-$H_2$) as a matrix host has generated considerable interest in recent years because of the unique properties of this quantum solid.[24−26] We have demonstrated that the diminished matrix cage effect makes feasible production of free radicals in solid *p*-$H_2$ via photolysis in situ of precursors or via photoinduced bimolecular reactions.[27−29] We extended this method to use electron bombardment during matrix deposition to produce protonated aromatic compounds and their neutral counterparts. We demonstrated several advantages of this method with the investigations of protonated benzene ($C_6H_7^+$) and the cyclohexadienyl radical (*c*-$C_6H_7$),[30] and protonated naphthalene (1-$C_{10}H_9^+$ and 2-$C_{10}H_9^+$) and their neutral counterparts;[31] the method is clean (with negligible fragmentation), sensitive, and enables high resolution and a wide spectral coverage as compared with other methods for spectral investigations of protonated aromatics. In this paper we report the IR absorption spectra of 1-pyridinium cations ($C_5H_5NH^+$) and pyridinyl radicals ($C_5H_5NH$ and 4-$C_5H_6N$) produced on electron bombardment of a mixture of $C_5H_5N$/*p*-$H_2$ during matrix deposition.

## 2. EXPERIMENTS

The experimental setup has been described previously.[28,30] A gold-plated copper substrate cooled to 3.2 K served also as a mirror to reflect the incident IR beam to the detector. IR absorption spectra were recorded with a Fourier-transform infrared (FTIR) spectrometer equipped with a KBr beamsplitter and Hg−Cd−Te detector (cooled to 77 K) to cover the spectral range 450−5000 cm$^{-1}$. Nine hundred scans at resolution 0.25 cm$^{-1}$ were generally recorded at each stage of the experiment.


dx.doi.org/10.1021/jp407668z | J. Phys. Chem. A 2013, 117, 13680−13690

**Table 1. Comparison of Observed Vibrational Wavenumbers ($cm^{-1}$) and Relative IR Intensities of Lines in Group $A^+$ with Harmonic and Anharmonic Vibrational Wavenumbers and Relative IR Intensities of $C_5H_5NH^+$ Predicted with the B3LYP/6-31++G(d,p) Method**

| | | calculations | | experiments | |
|---|---|---|---|---|---|
| mode | sym | harmonic[a] | anharmonic | $p$-$H_2$[a] | salts[b] |
| $\nu_1$ | $a_1$ | 3566 (100) | 3407 | 3381.9 (100) | 2375−3300 |
| $\nu_2$ | $a_1$ | 3252 (0) | 3122 | | |
| $\nu_3$ | $a_1$ | 3240 (7) | 3072 | 2929.3 (10) | 3040−3150 |
| $\nu_4$ | $a_1$ | 3222 (0) | 3086 | | |
| $\nu_5$ | $a_1$ | 1672 (22) | 1634 | 1634.7 (7) | 1631−1640 |
| $\nu_6$ | $a_1$ | 1520 (13) | 1489 | 1490.2 (14) | 1478−1490 |
| $\nu_7$ | $a_1$ | 1227 (1) | 1211 | | 1180−1207 |
| $\nu_8$ | $a_1$ | 1080 (2) | 1062 | | |
| $\nu_9$ | $a_1$ | 1046 (0) | 1029 | | |
| $\nu_{10}$ | $a_1$ | 1020 (2) | 1004 | | |
| $\nu_{11}$ | $a_1$ | 620 (0) | 613 | | |
| $\nu_{12}$ | $a_2$ | 1002 (0) | 993 | | |
| $\nu_{13}$ | $a_2$ | 880 (0) | 870 | | |
| $\nu_{14}$ | $a_2$ | 401 (0) | 397 | | |
| $\nu_{15}$ | $b_1$ | 1042 (0) | 1041 | | |
| $\nu_{16}$ | $b_1$ | 985 (1) | 976 | | |
| $\nu_{17}$ | $b_1$ | 850 (5) | 832 | | |
| $\nu_{18}$ | $b_1$ | 743 (58) | 736 | 735.1 (33) | 738−755 |
| $\nu_{19}$ | $b_1$ | 669 (54) | 671 | 666.5 (31) | 662−681 |
| $\nu_{20}$ | $b_1$ | 389 (0) | 385 | | |
| $\nu_{21}$ | $b_2$ | 3250 (13) | 3119 | 2965.4 (44) | 3040−3150 |
| $\nu_{22}$ | $b_2$ | 3238 (1) | 3104 | | |
| $\nu_{23}$ | $b_2$ | 1652 (21) | 1608 | 1607.9 (13) | 1600−1613 |
| $\nu_{24}$ | $b_2$ | 1577 (28) | 1543 | 1541.8 (22) | 1525−1542 |
| $\nu_{25}$ | $b_2$ | 1414 (2) | 1388 | | 1358−1378 |
| $\nu_{26}$ | $b_2$ | 1371 (6) | 1339 | 1330.1 (6) | 1318−1336 |
| $\nu_{27}$ | $b_2$ | 1297 (2) | 1277 | | 1235−1255 |
| $\nu_{28}$ | $b_2$ | 1198 (2) | 1186 | | |
| $\nu_{29}$ | $b_2$ | 1084 (3) | 1055 | | |
| $\nu_{30}$ | $b_2$ | 644 (0) | 638 | | |

[a]IR intensities as percent of that of most intense line near 3500 $cm^{-1}$ are listed in parentheses. The IR intensity of the line at 3566 $cm^{-1}$ is predicted to be 160.9 km $mol^{-1}$. Additional lines at 2938.3, 2911.8, and 2880.0 $cm^{-1}$ are assigned to the nonfundamental such as combination and/or overtone bands of $(2\nu_{19} + \nu_{23})$, $(\nu_{23} + \nu_{26})$, and $2\nu_6/(2\nu_{18} + \nu_{26})$, respectively. [b]Summary of results from various pyridinium salts.[16]

The protonated pyridine and its neutral counterpart were produced by electron bombardment during deposition of a gaseous sample of $p$-$H_2$ containing a small proportion of $C_5H_5N$. Typically, a mixture of $C_5H_5N/p$-$H_2$ (1/2500−1/3500) was deposited at a rate of 13 mmol $h^{-1}$ over a period of 4−8 h. An electron gun was used to generate an electron beam at 250 V and 55−65 $\mu$A to aim at the cold substrate during deposition. To differentiate various products produced under electron bombardment of $C_5H_5N/p$-$H_2$, we typically maintained the matrix in darkness for ∼15 h or performed secondary photolysis using light at 365 ± 10 nm from a light-emitting diode (375 mW) and at 405 nm from a diode laser (120 mW).

The $C_5H_6N$ radicals were produced also on irradiation of a $Cl_2/C_5H_5N/p$-$H_2$ matrix with ultraviolet (UV) light for 3 h followed by IR light for 0.5 h. The SiC source from the FTIR spectrometer served as a source of IR light. We have shown that these experimental procedures produce H atoms[30] because irradiation of $Cl_2$ molecules with light at 365 nm produces isolated Cl atoms[32] and subsequent IR irradiation of the matrix produces vibrationally excited $H_2$ that reacts with Cl to produce H atom and HCl. The H atoms thus produced subsequently react with pyridine to form $C_5H_6N$ radicals. Typically, a gaseous mixture of $C_5H_5N/p$-$H_2$ (1/3000−1/3500) and $Cl_2$ were codeposited with a flow rate ∼12 mmol $h^{-1}$ over a period of 10 h. The ratio of $Cl_2/C_5H_5N/p$-$H_2$ was approximately 1.8/1/3000. To differentiate further the absorption of various products, secondary photolysis was undertaken with light at 365 nm for 30 min. During UV photolysis and during acquisition of spectral data, an IR filter with cutoff wavelength at 2.4 $\mu$m was used to avoid the reaction between Cl and $p$-$H_2$.

The efficiency for conversion to $p$-$H_2$ was controlled by the temperature of the catalyst, typically ∼13 K, which gives a proportion of $o$-$H_2$ less than 100 ppm according to the Boltzmann distribution. Pyridine ($C_5H_5N$, Sigma-Aldrich, 99.8%) was vacuum distilled over KOH and degassed for a few minutes before use. $Cl_2$ (99.99%, AGA Specialty Gases) was used without further purification.

## 3. QUANTUM-CHEMICAL CALCULATIONS

Geometry optimizations and calculations of vibrational wavenumbers were performed using B3LYP hybrid functionals[33,34] and the 6-31++G(d,p) basis set. Algebraic first derivatives were utilized in the geometry optimization, and harmonic vibrational wavenumbers were calculated analytically at each stationary point. The anharmonic effects were calculated with a second-order perturbation approach using an effective finite-difference

Table 2. Comparison of Observed Vibrational Wavenumbers ($cm^{-1}$) and Relative IR Intensities of Lines in Group A with Harmonic and Anharmonic Vibrational Wavenumbers and Relative IR Intensities of $C_5H_5NH$ Predicted with the B3LYP/6-31++G(d,p) Method

| | | calculations | | experiments | |
|---|---|---|---|---|---|
| mode | sym | harmonic[a] | anharmonic | $p$-$H_2$ (e-impact)[a] | $p$-$H_2$ (H rx)[a] |
| $\nu_1$ | a′ | 3660 (64) | 3567 | 3493.1 (77) | 3493.1 (84) |
| $\nu_2$ | a′ | 3238 (0) | 3106 | | |
| $\nu_3$ | a′ | 3228 (14) | 3088 | | |
| $\nu_4$ | a′ | 3196 (1) | 3075 | | |
| $\nu_5$ | a′ | 1666 (3) | 1614 | | |
| $\nu_6$ | a′ | 1462 (2) | 1430 | | |
| $\nu_7$ | a′ | 1211 (0) | 1189 | | |
| $\nu_8$ | a′ | 1036 (1) | 1018 | | |
| $\nu_9$ | a′ | 989 (16) | 968 | 972.9 (20) | 972.9 (20) |
| $\nu_{10}$ | a′ | 961 (57) | 949 | 952.8 (54) | 952.9 (53) |
| $\nu_{11}$ | a′ | 923 (2) | 878 | | |
| $\nu_{12}$ | a′ | 690 (48) | 662 | 641.8 (33) | 641.7 (32) |
| $\nu_{13}$ | a′ | 618 (100) | 606 | 616.2 (100) | 616.0 (100) |
| $\nu_{14}$ | a′ | 615 (69) | 593 | 605.4 (57) | 605.5 (51) |
| $\nu_{15}$ | a′ | 577 (3) | 582 | | |
| $\nu_{16}$ | a′ | 272 (112) | ~218?[b] | | |
| $\nu_{17}$ | a′ | 196 (56) | ~408?[b] | | |
| $\nu_{18}$ | a″ | 3234 (16) | 3089 | | |
| $\nu_{19}$ | a″ | 3198 (23) | 3060 | | |
| $\nu_{20}$ | a″ | 1566 (0) | 1527 | | |
| $\nu_{21}$ | a″ | 1467 (36) | 1438 | 1447.9 (37) | 1447.9 (37) |
| $\nu_{22}$ | a″ | 1367 (5) | 1339 | 1346.2 (3) | 1346.2 (4) |
| $\nu_{23}$ | a″ | 1352 (76) | 1310 | 1311.6 (64) | 1311.4 (60) |
| $\nu_{24}$ | a″ | 1220 (1) | 1203 | | |
| $\nu_{25}$ | a″ | 1080 (4) | 1058 | | |
| $\nu_{26}$ | a″ | 1011 (3) | 969 | | |
| $\nu_{27}$ | a″ | 929 (0) | 894 | | |
| $\nu_{28}$ | a″ | 711 (1) | 684 | | |
| $\nu_{29}$ | a″ | 638 (1) | 635 | | |
| $\nu_{30}$ | a″ | 434 (0) | 423 | | |

[a]IR intensities as percent of that of the intense line near 610 $cm^{-1}$ ($\nu_{13}$) are listed in parentheses. The IR intensity of the line near 618 $cm^{-1}$ is predicted to be 73.4 km $mol^{-1}$. [b]Unreliable anharmonicity due to flat potential energy surfaces.

evaluation of the third and semidiagonal fourth derivatives. Some calculations were performed also with (1) the B3PW91 method that uses Becke's three-parameter hybrid exchange functionals and a correlation functional of Perdew and Wang[35] with a 6-311++G(2d,2p) basis set and (2) the MP2 (Møller–Plesset second-order perturbation) method[36] with an aug-cc-pVDZ basis set.[37] All calculations employed the Gaussian 09 programs.[38]

**3.1. Pyridinium ($C_5H_6N^+$) Cations.** Important structural parameters and relative energies predicted with the B3LYP/6-31++G(d,p) method for various isomers of $C_5H_6N^+$ are presented in Figure 1. A list of parameters of all isomers of $C_5H_6N^+$ is given in Table S1 (Supporting Information); a comparison of structural parameters of $C_5H_5NH^+$ predicted with various quantum-chemical methods is given in Table S2 (Supporting Information). The N-protonated form, 1-pyridinium ($C_5H_5NH^+$) cation, is predicted to be the most stable. The energies of 2-, 3-, and 4-$C_5H_6N^+$ relative to that of $C_5H_5NH^+$, corrected with ZPE (zero-point vibrational energy), are predicted to be 231, 204, and 254 kJ $mol^{-1}$ with the B3LYP/6-31++G(d,p) method; these values are slightly smaller than values 266, 238, and 287 kJ $mol^{-1}$ predicted with the MP2/6-311G(2d,p) method.[1]

The harmonic and anharmonic vibrational wavenumbers and IR intensities of $C_5H_5NH^+$ predicted with the B3LYP/6-31++G(d,p) method are listed in Table 1. Those of 2-, 3-, and 4-$C_5H_6N^+$ are listed in Table S3 (Supporting Information). A comparison of harmonic vibrational wavenumbers and IR intensities of $C_5H_5NH^+$ predicted with various computational methods is presented in Table S4 (Supporting Information).

**3.2. Pyridinyl Radicals ($C_5H_6N$).** Important structural parameters and relative energies of $C_5H_6N$ radicals predicted with the B3LYP/6-31++G(d,p) method are presented in Figure 2. An extended list of parameters of these pyridinyl radicals is given in Table S5 (Supporting Information). The 1-pyridinyl ($C_5H_5NH$) radical is predicted to be the most stable, with enthalpy of reaction $\Delta H^0 = -128.8$ kJ $mol^{-1}$ from H + $C_5H_5N$. The ZPE-corrected energies of 2-, 3-, and 4-$C_5H_6N$ relative to that of $C_5H_5NH$ are predicted to be 30, 28, and 32 kJ $mol^{-1}$ with the B3LYP/6-31++G(d,p) method. These values are similar to values 30 and 25 kJ $mol^{-1}$ predicted for 2- and 3-$C_5H_6N$ with the MP2/6-311G(2d,p) method; the energy of 4-$C_5H_6N$ was previously uninvestigated.[1]

The harmonic and anharmonic vibrational wavenumbers and IR intensities of $C_5H_5NH$ and 4-$C_5H_6N$ according to the B3LYP/6-31++G(d,p) method are listed in Tables 2 and 3,


dx.doi.org/10.1021/jp407668z | J. Phys. Chem. A 2013, 117, 13680−13690

Table 3. Comparison of Observed Vibrational Wavenumbers ($cm^{-1}$) and Relative IR Intensities of Lines in Group B with Harmonic and Anharmonic Vibrational Wavenumbers and Relative IR Intensities of 4-$C_5H_6N$ Predicted with the B3LYP/6-31++G(d,p) Method

| | | calculations | | experiments | |
|---|---|---|---|---|---|
| mode | sym | harmonic[a] | anharmonic | $p$-$H_2$ (e-impact)[a] | $p$-$H_2$ (H rx)[a] |
| $\nu_1$ | $a_1$ | 3195 (2) | 3043 | | |
| $\nu_2$ | $a_1$ | 3167 (25) | 3045 | | |
| $\nu_3$ | $a_1$ | 2936 (83) | 2823 | 2782.7 (34) | 2782.8 (35) |
| $\nu_4$ | $a_1$ | 1599 (17) | 1548 | 1553.2 (18) | 1553.2 (21) |
| $\nu_5$ | $a_1$ | 1459 (4) | 1428 | 1428.2 (13) | 1428.2 (10) |
| $\nu_6$ | $a_1$ | 1422 (32) | 1394 | 1376.5 (44) | 1376.5 (46) |
| $\nu_7$ | $a_1$ | 1222 (2) | 1197 | | |
| $\nu_8$ | $a_1$ | 1043 (6) | 1015 | | |
| $\nu_9$ | $a_1$ | 978 (45) | 960 | 961.9 (59) | 961.8 (61) |
| $\nu_{10}$ | $a_1$ | 892 (10) | 879 | | |
| $\nu_{11}$ | $a_1$ | 565 (7) | 558 | | |
| $\nu_{12}$ | $a_2$ | 1162 (0) | 1125 | | |
| $\nu_{13}$ | $a_2$ | 989 (0) | 968 | | |
| $\nu_{14}$ | $a_2$ | 747 (0) | 734 | | |
| $\nu_{15}$ | $a_2$ | 361 (0) | 352 | | |
| $\nu_{16}$ | $b_1$ | 2928 (33) | 2746 | 2737.3 (13) | 2737.3 (20) |
| $\nu_{17}$ | $b_1$ | 973 (1) | 949 | | |
| $\nu_{18}$ | $b_1$ | 912 (29) | 890 | 885.9 (33) | 885.7 (35) |
| $\nu_{19}$ | $b_1$ | 700 (98) | 688 | 685.9 (94) | 685.9 (90) |
| $\nu_{20}$ | $b_1$ | 532 (100) | 520 | 518.8 (100) | 518.8 (100) |
| $\nu_{21}$ | $b_1$ | 194 (0) | 190 | | |
| $\nu_{22}$ | $b_2$ | 3194 (146) | 3064 | | |
| $\nu_{23}$ | $b_2$ | 3165 (76) | 3035 | | |
| $\nu_{24}$ | $b_2$ | 1490 (89) | 1452 | 1452.6 (96) | 1452.5 (87) |
| $\nu_{25}$ | $b_2$ | 1421 (9) | 1388 | 1390.8 (6) | 1390.8 (9) |
| $\nu_{26}$ | $b_2$ | 1355 (7) | 1327 | | 1331.9? (7) |
| $\nu_{27}$ | $b_2$ | 1201 (21) | 1176 | | |
| $\nu_{28}$ | $b_2$ | 1131 (6) | 1112 | | |
| $\nu_{29}$ | $b_2$ | 979 (4) | 964 | | |
| $\nu_{30}$ | $b_2$ | 637 (18) | 630 | 623.5 (12) | 623.5 (12) |

[a]IR intensities as percent of that of the intense line near 532 $cm^{-1}$ are listed in parentheses. The IR intensity of the line near 532 $cm^{-1}$ is predicted to be 32.6 km $mol^{-1}$.

respectively. Those of 2-, 3-, and 4-$C_5H_6N$ are compared in Table S6 (Supporting Information).

The molecular electrostatic potential map and Mulliken atomic charges (in units of e, listed in parentheses) for individual atoms of $C_5H_5N$ computed with the B3PW91/6-311++G(2d,2p) method are shown in Figure 3. The predicted atomic charges on N, C1, C2, C3, and C4 atoms in $C_5H_5N$ are −0.257e, −0.129e, +0.012e, and −0.145e, respectively.

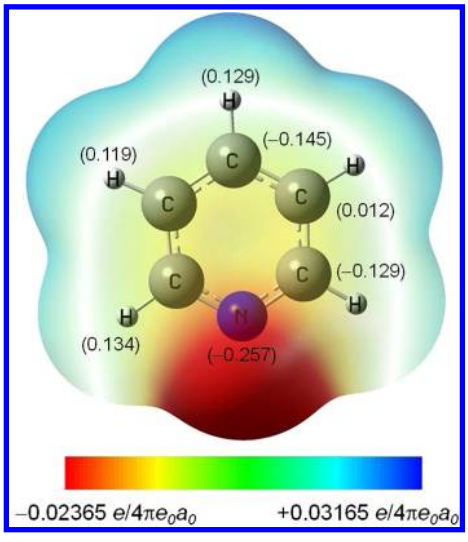


Figure 3. Molecular electrostatic potential of $C_5H_5N$ mapped onto 0.0004 e $Å^{-3}$ isosurface of the electron density predicted with the B3PW91/6-311++G(2d,2p) method. Individual Mulliken atomic charges (in units of e) on N, C, and H atoms are listed in parentheses.

## 4. EXPERIMENTAL RESULTS

### 4.1. Electron Bombardment on $C_5H_5N/p$-$H_2$ Mixtures.

The IR spectrum of a $C_5H_5N/p$-$H_2$ matrix exhibited intense lines at 3084.6, 3039.0, 3007.0, 1598.5, 1583.0, 1579.5, 1483.2, 1440.9, 1217.7, 1031.1, 991.3, 744.3, 701.7, and 601.9 $cm^{-1}$, as shown in Figure 4a of ref 39. The wavenumbers of these lines, listed in Table 1 of ref 39, agree with the reported spectra of gaseous $C_5H_5N$ (ref 40) and $C_5H_5N$ isolated in $N_2$ (refs 41 and 42) and Ar matrices.[43] When the $C_5H_5N/p$-$H_2$ mixture was bombarded with an e-gun during deposition, many new features appeared. The difference spectrum obtained by subtraction of the spectrum of a $C_5H_5N/p$-$H_2$ (1/3000) matrix from the spectrum of the electron bombarded $C_5H_5N/p$-$H_2$ (1/3000) mixture is presented in Figure 4a. To differentiate the absorption lines of positively charged species from those of the


dx.doi.org/10.1021/jp407668z | J. Phys. Chem. A 2013, 117, 13680−13690

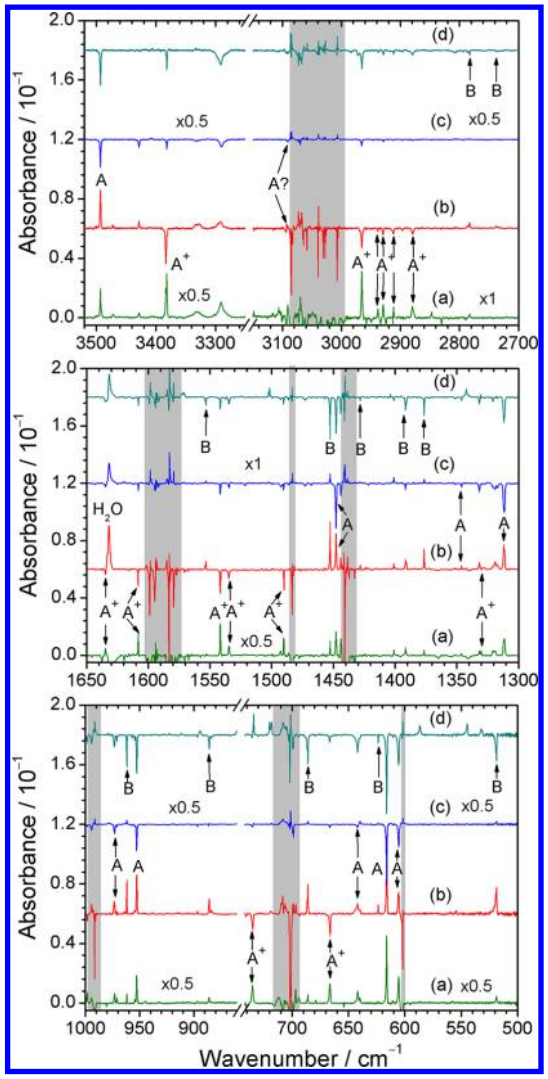


**Figure 4.** Difference spectra of (a) the $C_5H_5N/p\text{-}H_2$ (1/3000) mixture upon electron bombardment during deposition at 3.2 K for 6 h (lines of $C_5H_5N$ are stripped according to the spectrum of a $C_5H_5N/p\text{-}H_2$ (1/3000) matrix), (b) the sample after being maintained in darkness at 3.2 K for 15 h, (c) the sample upon irradiation at 365 nm for 40 min, and (d) the sample upon further irradiation at 405 nm for 30 min. The assignments of lines in each group are $A^+$, $C_5H_5NH^+$, A, $C_5H_5NH$, and B, 4-$C_5H_6N$. Spectral regions suffering from severe interference from absorption of $C_5H_5N$ are marked with light gray.

neutral ones, we maintained the matrix in darkness for 15 h to allow diffusion of trapped electrons to react with the cations in solid $p\text{-}H_2$. The resultant difference spectrum is shown in Figure 4b; lines pointing upward indicate production, whereas those pointing downward indicate destruction. Subsequently, we irradiated the matrix at 365 nm for ~40 min to release the trapped electrons to neutralize the cations in the $p\text{-}H_2$ matrix; photolysis of various species might also take place. The observed difference spectrum is shown in Figure 4c. Some experiments with secondary photolysis were also performed. In Figure 4d we show the difference spectrum of the matrix upon further irradiation at 405 nm for 30 min.

As shown in Figure 4b, lines at 3381.9, 2965.4, 2938.3, 2929.3, 2911.8, 2880.0, 1634.7, 1607.9, 1541.8, 1490.2, 1330.1, 735.1, and 666.5 cm$^{-1}$ decreased in intensity after maintaining the matrix in darkness for a prolonged period and upon further irradiation at 365 and 405 nm. These features, designated as group $A^+$, demonstrate a correlated change in intensity at various stages of experiments and in separate experiments. They are assigned to the 1-pyridinium ($C_5H_5NH^+$) cation, to be discussed in section 5.1. Observed wavenumbers and relative IR intensities of lines in group $A^+$ are compared with predicted values in Table 1. As the region 3000−3100 cm$^{-1}$ is severely interfered with by absorption of $C_5H_5N$, no line in this region can be positively identified and characterized.

The features pointing upward in Figure 4b are separated into two groups according to their behavior upon secondary photolysis. Lines at 3493.1, 1447.9, 1346.2, 1311.6, 972.9, 952.8, 641.8, 616.2, and 605.4 cm$^{-1}$ decreased in intensity significantly upon irradiation at 365 nm and only slightly upon irradiation at 405 nm; they are designated as group A and assigned to the 1-pyridinyl ($C_5H_5NH$) radical, to be discussed in section 5.2. Observed wavenumbers and relative IR intensities of lines in group A are compared with predicted values in Table 2.

The intensities of lines at 2782.7, 2737.3, 1553.2, 1452.6, 1428.2, 1390.8, 1376.5, 961.9, 885.9, 685.9, 623.5, and 518.8 cm$^{-1}$ that increased slightly upon irradiation of the sample at 365 nm but decreased significantly upon irradiation at 405 nm, are designated as group B and assigned to the 4-$C_5H_6N$ radical, to be discussed in section 5.2. Observed wavenumbers and relative IR intensities of lines in group B are compared with predicted values in Table 3.

The mixing ratios of the precursor and observed products were estimated using the method described by Ruzi et al.[44] Using the predicted IR intensities of several intense lines at 1490.2, 1541.8, and 3381.9 cm$^{-1}$ for $C_5H_5NH^+$, 616.2, 1447.9, and 3493.1 cm$^{-1}$ for $C_5H_5NH$, and 518.8, 685.9, 961.9, and 1452.6 cm$^{-1}$ for 4-$C_5H_6N$, we estimated the mixing ratios after deposition to be $[C_5H_5NH^+]$ = 2.0 ± 0.4 ppm, $[C_5H_5NH]$ = 2.6 ± 0.6 ppm, and $[4\text{-}C_5H_6N]$ = 0.85 ± 0.12 ppm. The variations in mixing ratio as a result of maintaining the sample in darkness for 15 h (Figure 4b) are $\Delta[C_5H_5NH^+]$ = −0.8 ± 0.2 ppm, $\Delta[C_5H_5NH]$ = 1.9 ± 0.5 ppm, and $\Delta[4\text{-}C_5H_6N]$ = 1.6 ± 0.3 ppm. Upon irradiation of the sample at 365 nm for 40 min (Figure 4c), $\Delta[C_5H_5NH^+]$ = −0.31 ± 0.04 ppm, $\Delta[C_5H_5NH]$ = −2.5 ± 0.7 ppm, and $\Delta[4\text{-}C_5H_6N]$ = 0.37 ± 0.05 ppm. Upon irradiation of the sample at 405 nm for 30 min (Figure 4d), $\Delta[C_5H_5NH^+]$ = −0.34 ± 0.02 ppm, $\Delta[C_5H_5NH]$ = −1.9 ± 0.5 ppm, $\Delta[4\text{-}C_5H_6N]$ = −1.6 ± 0.3 ppm.

**4.2. Photolysis of $Cl_2/C_5H_5N/p\text{-}H_2$ matrices.** After codeposition of $Cl_2$ and $C_5H_5N$ in $p\text{-}H_2$ we observed, in addition to lines of $C_5H_5N$, new features, intense at 3091.4, 3047.2, 1591.8, 1446.7, 1212.7, 1070.3, 1003.7, 746.2, 699.0, 616.2, and 458.4 cm$^{-1}$ that have been assigned to the σ-bonded $C_5H_5N{-}Cl_2$ complex.[39] Upon irradiation of the sample at 365 nm for 3 h, the intensities of lines of $C_5H_5N$ increased slightly and those of $C_5H_5N{-}Cl_2$ diminished and a set of new lines at 1449.7, 1200.6, and 688.7 cm$^{-1}$ due to $C_5H_5NCl$ appeared; as reported previously, because $C_5H_5NCl$ was also dissociated by light at 365 nm, these lines are weak.[39] Figure 5a shows a partial spectrum of the UV-irradiated $Cl_2/C_5H_5N/p\text{-}H_2$ (1.8/1/3000) sample; lines of $C_5H_5N$, $C_5H_5N{-}Cl_2$, and $C_5H_5N{-}HCl$ are marked with "o", "*", and "Δ", respectively. Broad and intense features at 1052.1 and 904.5 cm$^{-1}$ are due to the $C_5H_5N{-}HCl$ complex.[39,45] The matrix was subsequently irradiated with IR light for 30 min. The difference spectrum obtained on subtracting the spectrum in Figure 5a from the spectrum recorded after irradiation with IR light is presented in Figure 5b. New lines similar to those in groups A and B discussed in


dx.doi.org/10.1021/jp407668z | J. Phys. Chem. A 2013, 117, 13680−13690

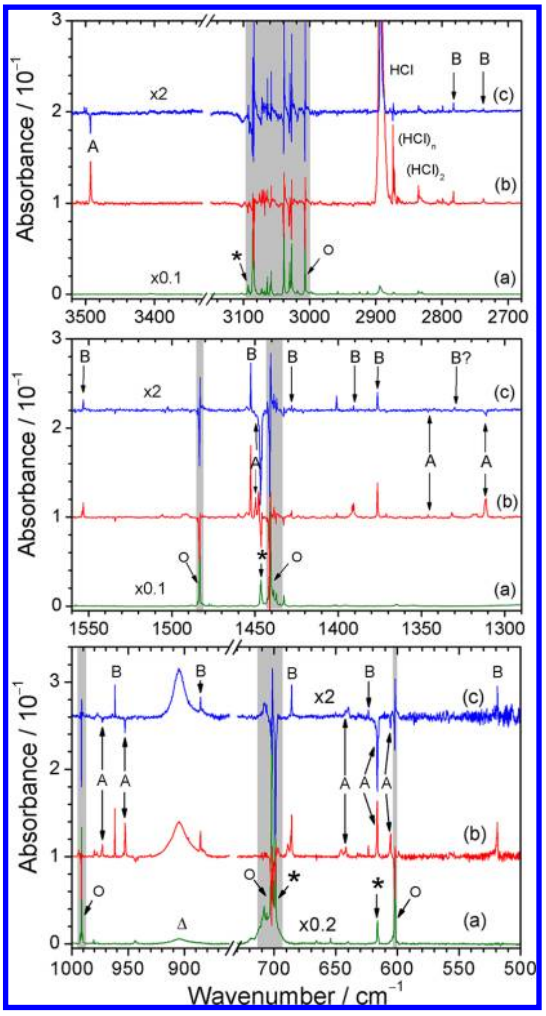


**Figure 5.** (a) Spectrum of the $Cl_2/C_5H_5N/p\text{-}H_2$ (1.8/1/3000) sample, deposited at 3.2 K for 10 h and irradiated at 365 nm for 3 h. Lines due to $C_5H_5N$, $C_5H_5N{-}Cl_2$, and $C_5H_5N{-}HCl$ complex are marked with "o", "*", and "Δ", respectively. Difference spectra of (b) the sample after subsequent irradiation with IR light for 30 min, and (c) the sample after further irradiation at 365 nm for 30 min. The assignments of lines in each group are A, $C_5H_5NH$, and B, 4-$C_5H_6N$. Spectral regions suffering from severe interference from absorption of $C_5H_5N$ are marked with light gray.

the preceding sections were observed. Upon secondary photolysis at 365 nm, intensities of lines in group A decreased, whereas those of lines in group B increased, as shown in Figure 5c. Lines of group A are indicated in Figure 5b,c and those of group B are indicated in Figure 5c.

Similarly to the description in the preceding section, we estimated the variation in mixing ratios after IR irradiation (Figure 5b) to be $\Delta[C_5H_5NH] = 2.4 \pm 0.4$ ppm and $\Delta[4\text{-}C_5H_6N] = 3.8 \pm 0.7$ ppm. The variation in mixing ratios after secondary photolysis at 365 nm (Figure 5c) was estimated to be $\Delta[C_5H_5NH] = -0.7 \pm 0.1$ ppm and $\Delta[4\text{-}C_5H_6N] = 1.0 \pm 0.2$ ppm.

Upon photolysis of the $Cl_2/C_5H_5N/p\text{-}H_2$ samples at 365 nm, weak lines near 2894, 2836, and 2873 $cm^{-1}$ appeared; these lines are due to HCl, $(HCl)_2$, and $(HCl)_n$, respectively.[46] Their intensities increased significantly when the matrix was irradiated with IR light because of the reaction between Cl and $H_2$.

## 5. DISCUSSION

**5.1. Assignment of Lines in Group $A^+$ to $C_5H_5NH^+$.** The observation of the decay of the lines assigned in group $A^+$ indicates that the most likely carrier of these lines is one of the four isomeric forms of pyridinium cations because the neutralization took place when the matrix sample was maintained in darkness for a prolonged period or irradiated with light at 365 nm. In Figure 6a we show the inverted spectrum of Figure 4b so that lines in group $A^+$ are pointing upward; regions of interference due to absorption of $C_5H_5N$ are shaded with light gray. In Figure 6b–e, we plot the simulated IR spectra of four isomers of pyridinium cations: $C_5H_5NH^+$ and 2-, 3-, and 4-$C_5H_6N^+$, respectively. These spectra were simulated according to the anharmonic vibrational wave-

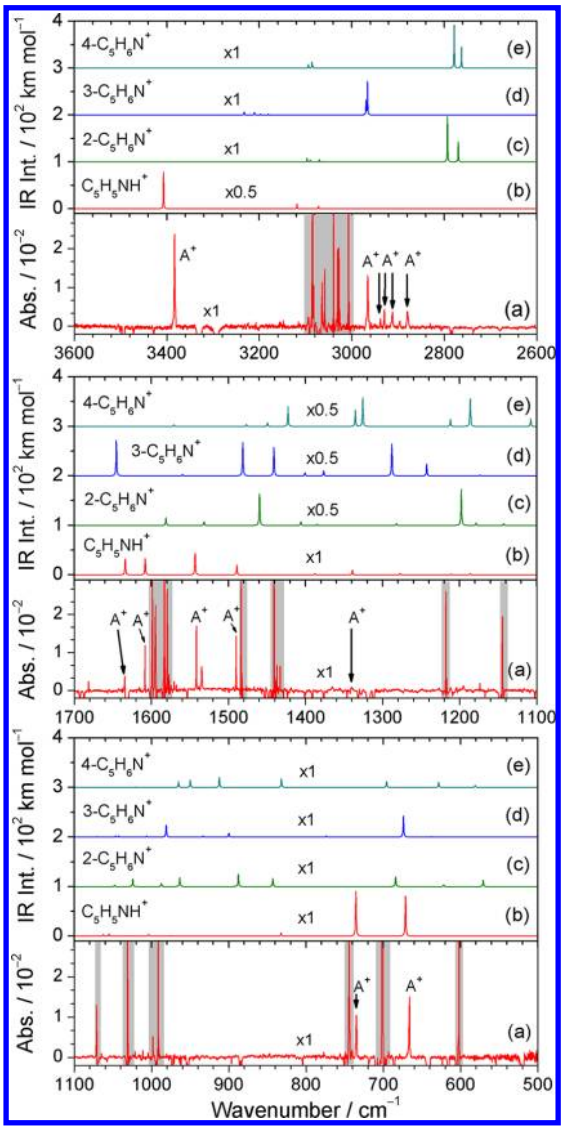


**Figure 6.** Comparison of experimental spectra with simulated spectra. (a) Inverted spectrum of Figure 4b, the difference spectrum of the electron-bombarded $C_5H_5N/p\text{-}H_2$ (1/3000) sample after being maintained in darkness at 3.2 K for 15 h. IR stick spectra of (b) $C_5H_5NH^+$, (c) 2-$C_5H_6N^+$, (d) 3-$C_5H_6N^+$, and (e) 4-$C_5H_6N^+$ simulated according to anharmonic vibrational wavenumbers and IR intensities predicted with the B3LYP/6-31++(d,p) method. Lines in group $A^+$ are assigned to $C_5H_5NH^+$. Spectral regions that suffer from severe interference from absorption of $C_5H_5N$ are marked with light gray.


dx.doi.org/10.1021/jp407668z | J. Phys. Chem. A 2013, 117, 13680–13690

numbers and IR intensities predicted with the B3LYP/6-31++G(d,p) method, listed in Table 1 and Table S3 (Supporting Information), and a spectral width of 0.5 $cm^{-1}$. All four spectra show distinct spectral patterns because the additional N−H or C−H bonding at various sites has distinct effects on the bonding of the aromatic ring.

The observed wavenumbers and relative IR intensities of lines agree satisfactorily with those calculated for the $C_5H_5NH^+$ cation, but not with any of the 2-, 3-, and 4-$C_5H_6N^+$ cations, as illustrated in Figure 6. Observed line positions and relative intensities of lines in group $A^+$ are compared with harmonic and anharmonic vibrational wavenumbers and relative IR intensities predicted for $C_5H_5NH^+$ with the B3LYP/6-31++G(d,p) method in Table 1. The calculated harmonic wavenumbers and relative IR intensities of $C_5H_5NH^+$ obtained with various methods[1,7,47] are compared in Table S4 (Supporting Information). The six most intense lines were observed at 3381.9, 1637.8, 1607.9, 1541.8, 735.1, and 666.5 $cm^{-1}$, near the anharmonic vibrational wavenumbers predicted at 3407 (NH stretch), 1634 (C═C stretch), 1608 (C═C and CN stretch), 1543 (CH in-plane bend), 736 (CH/NH out-of-plane bend mixed with ring out-of-plane deformation), and 671 (CH/NH out-of-plane bend mixed with out-of-plane ring deformation) $cm^{-1}$; the NH-stretching mode is characteristic of the structure of this cation. Assignments of lines at 2965.8 and 2929.2 $cm^{-1}$ in the CH-stretching region are tentative because the predicted anharmonic vibrational wavenumbers, 3119 and 3072 $cm^{-1}$, are slightly greater; the possibility that these two lines are due to some overtone or combination bands and these two CH-stretching lines are buried in the 3000−3100 $cm^{-1}$ region with which there is severe interference from absorption of pyridine cannot be positively excluded. The deviations between the calculated anharmonic vibrational wavenumbers and the observed wavenumbers are smaller than 0.7%, except lines tentatively assigned to the symmetric and antisymmetric CH-stretching ($\nu_3$ and $\nu_{21}$) modes, which show deviations ∼5%.

Most observed vibrational wavenumbers are similar to those reported for pyridinium salts $C_5H_5NH^+X^-$, in which $X^-$ is the counteranion;[16] the ranges of observed wavenumbers in various salts are listed in Table 1 for comparison. We observed a line at 3381.9 $cm^{-1}$ for the NH-stretching mode. This line is to the blue of the range 2375−3300 $cm^{-1}$ reported for this mode, consistent with the expectation that the N−H moiety of isolated $C_5H_5NH^+$ is free whereas that of the pyridinium salt interacts with the anion.

Considering the observed photolytic and chemical behavior, the agreement of wavenumber and relative IR intensity between lines observed in group $A^+$ and those predicted for the $C_5H_5NH^+$ radical, the absence of some unique features expected for the 2-, 3-, and 4-$C_5H_6N^+$ radicals, and the calculated thermochemistry, we assign these new features in group $A^+$ to the 1-pyridinium ($C_5H_5NH^+$) cation, the most stable isomer.

**5.2. Assignment of Lines in Groups A and B to the $C_5H_5NH$ and 4-$C_5H_6N$ Radicals.** The intensities of lines in group A increased after the e-impacted $C_5H_5N/p$-$H_2$ matrix was maintained in darkness for 15 h and decreased significantly upon irradiation at 365 nm, indicating that the carrier might be a neutral species that dissociates at 365 nm. The intensities of lines in group B increased after the sample was maintained in darkness and upon irradiation at 365 nm but decreased significantly upon irradiation at 405 nm, indicating that the carrier might be a neutral species that dissociates at 405 nm. Both these features were observed also in experiments of $Cl_2/C_5H_5N/p$-$H_2$ irradiated with UV and IR light, in which reactions of H with $C_5H_5N$ are expected and no ion can be produced. We hence expect that the carriers of lines in groups A and B are likely the isomers of $C_5H_6N$ radicals.

In Figure 7a we reproduce the spectrum of Figure 4b, the difference spectrum recorded on maintaining the e-impacted $C_5H_5N/p$-$H_2$ matrix in darkness for 15 h. In Figure 7b we reproduce the spectrum of Figure 5c, the difference spectrum upon secondary irradiation at 365 nm of the $Cl_2/C_5H_5N/p$-$H_2$ matrix that was previously irradiated with UV and IR light. Lines in group A (pointing upward in Figure 7a and pointing

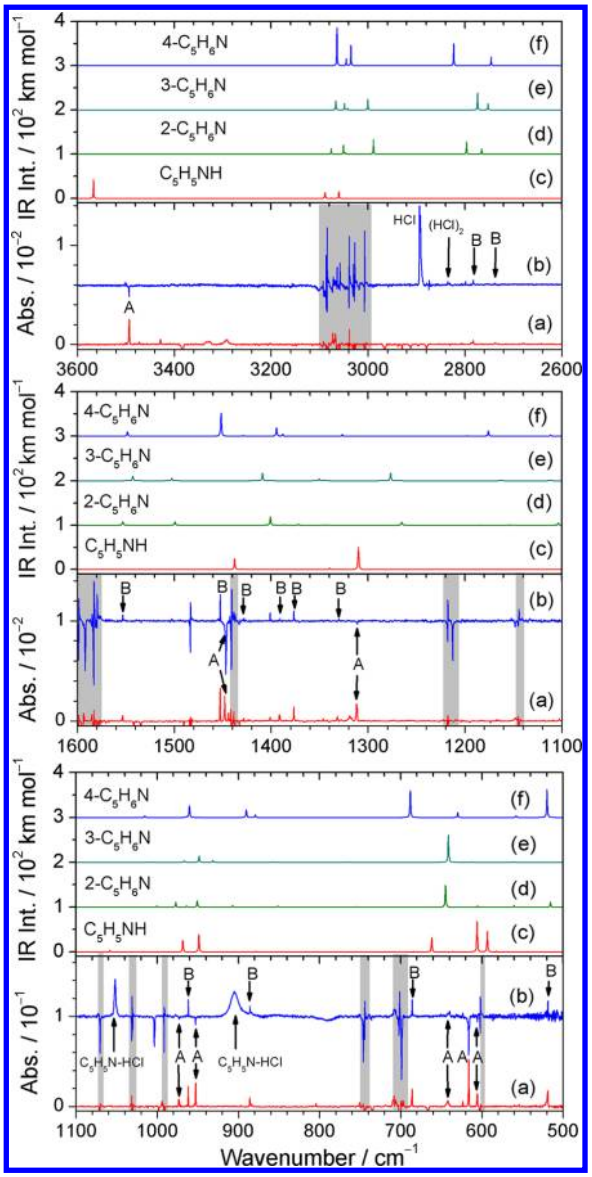


**Figure 7.** Comparison of experimental spectra with simulated spectra. (a) Spectrum reproduced from Figure 4b and (b) spectrum reproduced from Figure 5c. IR stick spectrum of (c) $C_5H_5NH$, (d) 2-$C_5H_6N$, (e) 3-$C_5H_6N$, and (f) 4-$C_5H_6N$ simulated according to anharmonic vibrational wavenumbers and IR intensities predicted with the B3LYP/6-31++(d,p) method. Lines in groups A and B are assigned to $C_5H_5NH$ and 4-$C_5H_6N$, respectively. Spectral regions that suffer from severe interference from absorption of $C_5H_5N$ are marked with light gray.


dx.doi.org/10.1021/jp407668z | J. Phys. Chem. A 2013, 117, 13680−13690

downward in Figure 7b) and B (pointing upward in Figure 7a,b) are marked; regions of interference due to absorption of $C_5H_5N$ are marked with light gray.

In Figure 7c–f, we plot simulated IR spectra of four possible isomers of pyridinyl radicals: $C_5H_5NH$, 2-, 3-, and 4-$C_5H_6N$, respectively; the spectra were simulated according to the anharmonic vibrational wavenumbers and IR intensities predicted with the B3LYP/6-31++(d,p) method, listed in Table 2 and Table S6 (Supporting Information), and a spectral width of 0.5 $cm^{-1}$. Similar to the case of $C_5H_6N^+$, the spectral patterns of all four spectra are distinct because the additional N–H or C–H bonding at various sites has varied effects on the bonding of the aromatic ring.

The observed wavenumbers and relative IR intensities of lines in group A agree satisfactorily with those calculated for the $C_5H_5NH$ radical, but not with any of the 2-, 3-, and 4-$C_5H_6N$ radicals, as illustrated in Figure 7. The observed positions and relative intensities of lines in group A are compared with harmonic and anharmonic vibrational wavenumbers and relative IR intensities predicted for $C_5H_5NH$ with the B3LYP/6-31++G(d,p) method in Table 2. The five most intense lines were observed at 3493.1, 1311.6, 952.8, 616.2, and 605.4 $cm^{-1}$, near the anharmonic vibrational wavenumbers predicted at 3567 (NH-stretch), 1310 (CCC and CNC asymmetric stretch), 949 (CNC symmetric stretch), 606 (CH out-of-plane bend mixed with ring out-of-plane deformation), and 593 (CH out-of-plane bend) $cm^{-1}$. The NH-stretching mode near 3490 $cm^{-1}$ is characteristic of $C_5H_5NH$. It is slightly greater than the value 3381.9 $cm^{-1}$ observed for $C_5H_5NH^+$, indicating a slightly stronger N–H bonding, consistent with a predicted N–H bond length (1.008 Å) smaller than that (1.017 Å) of $C_5H_5NH^+$. Assignments in the CH-stretching region are difficult because of severe overlap with $C_5H_5N$. The observed deviations between calculated anharmonic wavenumbers and observed line positions are less than 0.7% for most observed lines, with the largest deviation of 3.0% for $\nu_{12}$.

The observed wavenumbers and relative IR intensities of lines in group B agree satisfactorily with those calculated for the 4-$C_5H_6N$ radical, but not with any of the $C_5H_5NH$, 2-$C_5H_6N$, and 3-$C_5H_6N$ radicals, as illustrated in Figure 7. The five most intense lines were observed at 2782.4, 1452.6, 961.9, 685.9, and 518.8 $cm^{-1}$, near the anharmonic vibrational wavenumbers predicted at 2823 ($CH_2$ symmetric stretch), 1452 (out-of-phase CC stretch), 960 (out-of-phase CNC and CCC bends), 688 (CH out-of-plane bend), and 520 ($CH_2$ rock mixed with CNC out-of-plane deform) $cm^{-1}$. The small (2782.4 and 2737.3 $cm^{-1}$) CH-stretching frequencies and the intense $CH_2$ rocking mode (518.8 $cm^{-1}$) are characteristic of the $\sigma$-bonded $C_5H_6N$ having a $CH_2$ moiety. Assignments in the CH-stretching region are difficult because of severe overlap with $C_5H_5N$; we hence are unable to identify the two intense lines near 3064 and 3035 $cm^{-1}$ predicted by theory. The observed deviations between calculated anharmonic wavenumbers and observed line positions are less than 0.4% for most observed lines, with the largest deviations of ~1.4% for the $CH_2$-stretching modes.

Although the H atoms produced in experiments of both types are expected to be small and the reaction of $C_5H_6N$ with the second H is less likely, for completeness we predicted the vibrational wavenumbers of dihydrogenated pyridines ($C_5H_7N$) for comparison. In Table S7 (Supporting Information) we list the vibrational wavenumbers and relative IR intensities calculated for 1,2-$C_5H_7N$, 1,3-$C_5H_7N$, and 1,4-$C_5H_7N$. These predicted spectra of isomers of $C_5H_7N$ agree with those observed for lines in neither group A nor B.

Considering the observed photolytic and chemical behavior, the agreement of wavenumber and relative IR intensity between lines observed in group A and predicted for the $C_5H_5NH$ radical, the absence of some unique features predicted for 2-, 3-, and 4-$C_5H_6N$, and the calculated thermochemistry, we assign the observed new features in group A to the 1-pyridinyl ($C_5H_5NH$) radical, the most stable isomer. We analogously assign the observed new features in group B to the 4-pyridinyl (4-$C_5H_6N$) radical.

**5.3. Formation Mechanism in *p*-$H_2$.** Ionization of $H_2$ by electron impact produces $H_2^+$; subsequent rapid exothermic proton transfer,

$$H_2^+ + H_2 \rightarrow H_3^+ + H \quad (1)$$

produces H and $H_3^+$.[48] The $H_3^+$ thus produced can readily transfer a proton to $C_5H_5N$ to form $C_5H_6N^+$,

$$H_3^+ + C_5H_5N \rightarrow C_5H_6N^+ + H_2 \quad (2)$$

We believe that these reactions took place mainly on the surface of *p*-$H_2$ because electron bombardment after deposition produced protonated species in much less amount.

The enthalpies of reaction for the formation of $C_5H_5NH^+$ and 2-, 3-, and 4-$C_5H_6N^+$ at 0 K are predicted to be −534, −290, −316, and −265 kJ $mol^{-1}$, respectively, with the B3LYP/6-31++G(d,p) method. Our observation of protonated pyridine as $C_5H_5NH^+$, but not 2-, 3-, or 4-$C_5H_6N^+$, agrees with the prediction that $C_5H_5NH^+$ is much more stable than the C-protonated isomers. The barrier from the most stable isomer $C_5H_5NH^+$ to form 2-$C_5H_6N^+$ is predicted to be ~276 kJ $mol^{-1}$, smaller than the exothermicity of the proton transfer in the reaction $H_3^+ + C_5H_5N \rightarrow C_5H_5NH^+ + H_2$. We observed no line of 2-$C_5H_6N^+$ or 3-$C_5H_6N^+$ or 4-$C_5H_6N^+$, presumably because the excess energy in $C_5H_5NH^+$ upon proton transfer from $H_3^+$ to $C_5H_5N$ was rapidly quenched.

The pyridinyl radicals, $C_5H_6N$, are expected to be formed in neutralization of pyridinium cations or in reactions between the H atom and pyridine:

$$C_5H_5NH^+ + e^- \rightarrow C_5H_5NH \quad (3)$$

$$C_5H_5N + H \rightarrow C_5H_6N \quad (4)$$

The enthalpies of reaction 4 at 298 K for the formation of $C_5H_5NH$ and 2-, 3-, and 4-$C_5H_6N$ are predicted to be −129, −100, −102, and −98 kJ $mol^{-1}$ with the B3LYP/6-31++G(d,p) method; the corresponding barriers were predicted to be 7.5, 17.2, 16.1, and 18.0 kJ $mol^{-1}$, respectively, similar to those predicted with the B3LYP/6-311+G(d,p)//B3LYP/6-31G(d) method.[49]

The observation of the $C_5H_5NH$ radical in experiments of electron bombardment of $C_5H_5N$/*p*-$H_2$ matrices is consistent with a theoretical prediction that $C_5H_5NH$ is the most stable isomer of pyridinyl radicals; the neutralization of the only observed isomer of protonated pyridine, $C_5H_5NH^+$, leads to only $C_5H_5NH$. In experiments with UV/IR irradiation of $Cl_2$/$C_5H_5N$/*p*-$H_2$ matrices, the observation of the $C_5H_5NH$ radical is consistent with a theoretical prediction that the formation of $C_5H_5NH$ via reaction 4 has the least barrier; considering the errors in predicting this small barrier (8 ± 4 kJ $mol^{-1}$) and the excess energy that the H atom might have after the reaction Cl + $H_2$ ($v$ = 1) → HCl + H in solid *p*-$H_2$ at 3.2 K, the formation of $C_5H_5NH$ via reaction 4 is likely to occur.


dx.doi.org/10.1021/jp407668z | J. Phys. Chem. A 2013, 117, 13680–13690

The reason that among all C-monohydrogenated pyridines only 4-$C_5H_6N$, not 2- or 3-$C_5H_6N$, was preferentially formed from both electron bombardment and H-reaction experiments is unclear. The three isomers 2-, 3-, and 4-$C_5H_6N$ were predicted to have similar energies and similar barrier heights for formation from H + $C_5H_5N$, with those for formation of 4-$C_5H_6N$ being the largest. One would expect that all three isomers would be formed from reaction 4. One possible reason is that the charge density of C4 predicted with the B3PW91/6-311++G(2d,2p) method is more negative than that of C3 and C2, as shown in Figure 3, so that the electrophilic H atom might prefer to attack the C4 atom to form 4-$C_5H_6N$. However, this tendency should be reflected in the reaction barrier. More sophisticated theoretical calculations on the reaction H + $C_5H_5N$, the interconversion among isomers of $C_5H_6N$, and reactions of H + $C_5H_6N$ are needed to explain our observations.

## 6. CONCLUSION

Electron bombardment was applied during the deposition of a mixture of $C_5H_5N$ and excess *p*-$H_2$ at 3.2 K to generate $C_5H_5NH^+$, $C_5H_5NH$, and 4-$C_5H_6N$ in the *p*-$H_2$ matrix. The intensities of lines of $C_5H_5NH$ and 4-$C_5H_6N$ radicals increased upon maintaining the matrix in darkness for a prolonged period, whereas those of $C_5H_5NH^+$ decreased. The formation of $C_5H_5NH$ and 4-$C_5H_6N$ radicals was observed also in experiments in which a $Cl_2$/$C_5H_5N$/*p*-$H_2$ matrix was irradiated with light at 365 nm and in the IR region to generate H atoms for reaction with $C_5H_5N$. Secondary photolysis at 365 nm at the initial stage diminished $C_5H_5NH$ but enhanced 4-$C_5H_6N$, whereas photolysis at 405 nm diminished 4-$C_5H_6N$ significantly.

The spectra were assigned according to the expected chemistry, the predicted exothermicity and energy barriers for possible reactions, and comparison with the anharmonic vibrational wavenumbers and IR intensities predicted with the B3LYP/6-31++G(d,p) method. The formation of $C_5H_5NH^+$ and $C_5H_5NH$ is consistent with theoretical predictions indicating that they are the most stable among all isomers, whereas the formation of 4-$C_5H_6N$ but not 2-$C_5H_6N$ or 3-$C_5H_6N$ is inexplicable with the current theoretically predicted barriers and enthalpies of formation of possible reactions but might be explained by the charge density over the C4 atom that is more negative than those of the C2 and C3 atoms so that the H atom might attack C4 more favorably. More sophisticated computations are needed to explain the observed selectivity.

## ■ ASSOCIATED CONTENT

### Supporting Information

Geometric parameters of all isomers of $C_5H_6N^+$ optimized with the B3LYP/6-31++G(d,p) method, comparison of parameters of $C_5H_5NH^+$ predicted with various methods, harmonic and anharmonic vibrational wavenumbers and IR intensities of 2-, 3-, 4-$C_5H_6N^+$ cations, comparison of harmonic vibrational wavenumbers and IR intensities of $C_5H_5NH^+$ predicted with various methods, geometric parameters of all isomers of $C_5H_6N$, harmonic and anharmonic vibrational wavenumbers and IR intensities of 2-, 3-, 4-$C_5H_6N$ radicals, harmonic and anharmonic vibrational wavenumbers and IR intensities of various isomers of $C_5H_7N$ radicals (Tables S1−S7). This material is available free of charge via the Internet at http://pubs.acs.org."

## ■ AUTHOR INFORMATION


### Corresponding Author

*Y.-P. Lee: e-mail, yplee@mail.nctu.edu.tw.


### Notes

The authors declare no competing financial interest.

## ■ ACKNOWLEDGMENTS

The National Science Council of Taiwan (Grant No. NSC101-2745-M009-001-ASP) and the Ministry of Education, Taiwan ("Aim for the Top University Plan" of National Chiao Tung University) supported this work. The National Center for High-performance Computing provided computer time.

## ■ REFERENCES


(1) Nguyen, V. Q.; Tureček, F. Gas-phase Protonation of Pyridine. A Variable-time Neutralization-Reionization and *ab initio* study of Pyridinium Radicals. *J. Mass. Spectrom.* **1997**, *32*, 55−63.

(2) Eisele, F. L.; McDaniel, E. W. Mass Spectrometry Study of Tropospheric Ions in the Northeastern and Southwestern United States. *J. Geophys. Res., [Atmos.]* **1986**, *91*, 5183−5188.

(3) Eisele, F. L. Natural and Transmission Line Produced Positive Ions. *J. Geophys. Res., [Atmos.]* **1989**, *94*, 6309−6318.

(4) Tanner, D. J.; Eisele, F. L. Ions in Oceanic and Continental Air Masses. *J. Geophys. Res., [Atmos.]* **1991**, *96*, 1023−1031.

(5) Joule, J. A.; Mills, K. *Heterocyclic Chemistry*, 5th ed.; Blackwell Publishing: Chichester, U.K., 2010.

(6) Vaganova, E.; Wachtel, E.; Leitus, G.; Danovich, D.; Lesnichin, S.; Shenderovich, I. G.; Limbach, H.; Yitzchaik, S. Photoinduced Proton Transfer in a Pyridine Based Polymer Gel. *J. Phys. Chem. B* **2010**, *114*, 10728−10733.

(7) Lee, I. C.; Masel, R. I. Evidence for Pyridinium Cation Formation during Coadsorption of Pyridine and Hydrogen on (2 × 1) Pt(110). *J. Phys. Chem. B* **2002**, *106*, 368−373.

(8) Bratile, K. M.; Komvopoulos, K.; Somorjai, G. A. Sum Frequency Generation Vibrational Spectroscopy of Pyridine Hydrogenation on Platinum Nanoparticles. *J. Phys. Chem. C* **2008**, *112*, 11865−11868.

(9) Parry, E. P. An Infrared Study of Pyridine Adsorbed on Acidic Solids−Characterization of surface acidity. *J. Catal.* **1963**, *2*, 371−379.

(10) Paukshtis, E. A.; Karakchiev, L. G.; Kotsarenko, N. S. IR-spectroscopic Study of Mechanism of Pyridine Protomation on the Surface of HNaY Zeolite. *React. Kinet. Catal. Lett.* **1977**, *6*, 147−152.

(11) Lias, S. G.; Liebman, J. F.; Levin, R. D. Evaluated Gas Phase Basicities and Proton Affinities of Molecules; Heats of Formation of Protonated Molecules. *J. Phys. Chem. Ref. Data* **1984**, *13*, 695−809.

(12) Hunter, E. P. L.; Lias, S. G. Evaluated Gas Phase Basicities and Proton Affinities of Molecules: An Update. *J. Phys. Chem. Ref. Data.* **1998**, *27*, 413−657.

(13) Hillebrand, C.; Klessinger, M.; Eckert-Maksić, M.; Maksić, Z. B. Theoretical Model Calculations of the Proton Affinities of Amino-alkanes, Aniline, and Pyridine. *J. Phys. Chem.* **1996**, *100*, 9698−9702.

(14) Ebrahimi, A.; Habibi-Khorasani, S. M.; Johantab, M. Additivity of Substituent Effects on the Proton Affinity and Gas-phase Basicity of Pyridines. *Comput. Theor. Chem.* **2011**, *966*, 31−37.

(15) Spinner, E. The Electronic Spectra of Some Monosubstituted Pyridines and Pyridinium Ions. *J. Chem. Soc.* **1963**, 3855−3859.

(16) Cook, D. Vibrational Spectra of Pyridinium Salts. *Can. J. Chem.* **1961**, *39*, 2009−2024.

(17) Foglizzo, R.; Novak, A. Spectres de Vibration de Quelques Halogenures de Pyridinium. *J. Chim. Phys.* **1969**, *66*, 1539−1550.

(18) Glazunov, V. P.; Odinokov, S. E. Infrared Spectra of Pyridinium Salts in Solution-II. Fermi Resonance and Structure of $\nu$NH Bands. *Spectrochim. Acta A* **1982**, *38*, 409−415.

(19) Gabes, W.; Stufkens, D. J.; Gerding, H. Structures, Raman, Infrared and Electronic Adsorption Spectra of Pyridinium Trihalides. *J. Mol. Struct.* **1973**, *17*, 329−340.

(20) Kotrla, J.; Florián, J.; Kubelková, L.; Fraissard, J. Pyridinium Ions-New Probe for Basic of Solid Acids. *Collect. Czech. Chem. Commun.* **1995**, *60*, 393−402.
(21) Farmer, V. C.; Mortland, M. M. An Infrared Study of the Co-ordination of Pyridine and Water to Exchangeable Cations in Montmorillonite and Saponite. *J. Chem. Soc. A* **1966**, 344−351.
(22) Cercek, B.; Ebert, M. Pulse Radiolysis Studies of the Reaction of H and OH Radicals and Hydrated Electrons with Pyridine. *Trans. Faraday Soc.* **1967**, *63*, 1687−1698.
(23) Fessenden, R. W.; Neta, P. ESR Spectra of Radicals Produced by Reduction of Pyridine and Pyrazine. *Chem. Phys. Lett.* **1973**, *18*, 14−17.
(24) Momose, T.; Shida, T. Matrix-Isolation Spectroscopy Using Solid Parahydrogen as Matrix: Application to High-Resolution Spectroscopy, Photochemistry, and Cryochemisty. *Bull. Chem. Soc. Jpn.* **1998**, *71*, 1−15.
(25) Yoshioka, T.; Raston, P. L.; Anderson, D. T. Infrared Spectroscopy of Chemically Doped Solid Parahydrogen. *Int. Rev. Phys. Chem.* **2006**, *25*, 469−496.
(26) Lee, Y.-P.; Wu, Y.-J.; Lees, R. M.; Xu, L.-H.; Hougen, J. T. Internal Rotation and Spin Conversion of $CH_3OH$ in Solid *Para*-Hydrogen. *Science* **2006**, *311*, 365−368.
(27) Bahou, M.; Lee, Y.-P. Diminished Cage Effect in Solid *p*-H2: Infrared Absorption of $CH_3S$ Observed from Photolysis *in situ* of $CH_3SH$, $CH_3SCH_3$, or $CH_3SSCH_3$ Isolated in *p*-$H_2$ Matrices. *J. Chem. Phys.* **2010**, *133*, 164316/1−164316/10.
(28) Amicangelo, J.; Lee, Y.-P. Site-Selective Reaction of Cl+ Propene in Solid *Para*-Hydrogen: Formation of 2-Chloropropyl Radicals. *J. Phys. Chem. Lett.* **2010**, *1*, 2956−2961.
(29) Lee, Y.-F.; Lee, Y.-P. Infrared Absorption of $CH_3SO_2$ Observed Upon Irradiation of a *p*-$H_2$ Matrix Containing $CH_3I$ and $SO_2$. *J. Chem. Phys.* **2011**, *134*, 124314/1−124314/8.
(30) Bahou, M.; Wu, Y.-J.; Lee, Y.-P. A New Method for Investigating Infrared Spectra of Protonated Benzene ($C_6H_7^+$) and Cyclohexadienyl Radical (*c*-$C_6H_7$) Using *Para*-Hydrogen. *J. Chem. Phys.* **2012**, *136*, 154304/1−154304/8.
(31) Bahou, M.; Wu, Y.-J.; Lee, Y.-P. Formation and Infrared Absorption of Protonated Naphthalenes (1-$C_{10}H_9^+$ and 2-$C_{10}H_9^+$) and Their Neutral Counterparts in Solid *Para*-Hydrogen. *Phys. Chem. Chem. Phys.* **2013**, *15*, 1907−1917.
(32) Raston, P. L.; Anderson, D. T. Infrared-induced Reaction of Cl Atoms Trapped in Solid Parahydrogen. *Phys. Chem. Chem. Phys.* **2006**, *8*, 3124−3129.
(33) Becke, A. D. Densityfunctional Thermochemistry. III. The Role of Exact Exchange. *J. Chem. Phys.* **1993**, *98*, 5648−5652.
(34) Lee, A.; Yang, W.; Parr, R. G. Development of the Colle-Salvetti Correlation-Energy Formula into a Functional of the Electron Density. *Phys. Rev. B* **1988**, *37*, 785−789.
(35) Perdew, J. P.; Burke, K.; Wang, Y. Generalized Gradient Approximation for the Exchange-correlation Hole of a Many-electron System. *Phys. Rev. B* **1996**, *54*, 16533−16539.
(36) Møller, C.; Plesset, M. S. Note on an Approximation for Many-Electron Systems. *Phys. Rev.* **1934**, *46*, 618−622.
(37) Dunning, T. H. Gaussian Basis Sets for Use in Correlated Molecular Calculations. I. The Atoms Boron through Neon and Hydrogen. *J. Chem. Phys.* **1989**, *90*, 1007−1023.
(38) Frisch, M. J.; Trucks, G. W.; Schlegel, H. B.; et al. *GAUSSIAN 09*, Revision A.02; Gaussian, Inc.: Wallingford, CT, USA, 2009.
(39) Das, P.; Bahou, M.; Lee, Y.-P. Reactions between Atomic Chlorine and Pyridine in Solid *Para*-Hydrogen: Infrared Spectrum of the 1-Chloropyridiny ($C_5H_5N$−Cl) radical. *J. Chem. Phys.* **2013**, *138*, 054307/1−054307/10.
(40) Wong, K. N.; Colson, S. D. The FT-IR Spectra of Pyridine and Pyridine-$d_5$. *J. Mol. Spectrosc.* **1984**, *104*, 129−151.
(41) Castellucci, E.; Sbrana, G.; Verderame, F. D. Infrared Spectra of Crystalline and Matrix Isolated Pyridine and Pyridine-$d_5$. *J. Chem. Phys.* **1969**, *51*, 3762−3770.
(42) Morris, V. R.; Bhatia, S. C.; Stelson, A. W.; Hall, J. H., Jr. Matrix-Isolation Study of the Thermal Decomposition of Pyridine. *Energy Fuels* **1991**, *5*, 126−133.
(43) Destexhe, A.; Smets, J.; Adamowicz, L.; Maes, G. Matrix Isolation FT-IR Studies and *ab Initio* Calculations of Hydrogen-Bonded Complex of Molecules Modeling Cytosine or Isocytosine Tautomers. 1. Pyridine and Pyrimidine Complexes with $H_2O$ in Ar Matrices. *J. Phys. Chem.* **1994**, *98*, 1506−1514.
(44) Ruzi, M.; Anderson, D. T. Photodissociation of N-methylformamide Isolated in Solid Parahydrogen. *J. Chem. Phys.* **2012**, *137*, 194313/1−194313/11.
(45) Szczepaniak, K.; Chabrier, P.; Person, W. B.; Del Bene, J. E. Experimental Infrared Spectra of Matrix Isolated Complexes of HCl with 4-Substituted Pyridines. Evaluation of Anharmonicity and Matrix Effects Using Data from *ab Initio* Calculations. *J. Mol. Struct.* **2000**, *520*, 1−18.
(46) Anderson, D. T.; Hinde, R. J.; Tam, S.; Fajardo, M. E. High-resolution Spectroscopy of HCl and DCl Isolated is Solid Parahydrogen: Direct, Induced, and Cooperative Infrared Transitions in a Molecular Quantum Solid. *J. Chem. Phys.* **2002**, *116*, 594−607.
(47) Szczepaniak, K.; Chabrier, P.; Person, W. B.; Del Bene, J. E. *Ab Initio* Theoretical and Matrix Isolation Experimental Studies of Hydrogen Bonding IV. The HBr:Pyridine Complex. *J. Mol. Struct.* **1997**, *436*−*437*, 367−386.
(48) Chan, M.-C.; Okumura, M.; Oka, T. Infrared Spectrum of p-Hydrogen Crystals Ionized by 3 MeV Electrons: Cluster Ions of Hydrogen in Condensed Phase. *J. Phys. Chem. A* **2000**, *104*, 3775−3779.
(49) Barckholtz, C.; Barckholtz, T. A.; Hadad, C. M. A Mechanistic Study of the Reactions of H, O($^3$P), and OH with Monocyclic Aromatic Hydrocarbons by Density Functional Theory. *J. Phys. Chem. A* **2001**, *105*, 140−152.